Original Research

S. Garré*
M. Javaux
J. Vanderborght
L. Pagès
H. Vereecken

The depletion of soil water by barley plants cropped on an undisturbed soil monolith was measured with electrical resistance tomography (ERT). The soil water content derived with ERT was compared at specific locations with TDR probes. A global water balance on the monolith and the comparison to TDR validated the ERT measurements.

S. Garré, M. Javaux, J. Vanderborght, and H. Vereecken, Forschungszentrum Jülich GmbH, Agrosphere (IBG-3), 52425 Jülich, Germany; M. Javaux, Earth and Life Institute/Environmental Sciences, Université catholique de Louvain, Croix du Sud 2, bte 2. 1348 Louvain-la-Neuve, Belgium; L. Pagès, UR 1115 Plantes et Systèmes de culture Horticoles INRA, Site Agroparc, 84914 Avignon Cedex 9, France. *Corresponding author (sarah.garre@ees.kuleuven.be).

Vadose Zone J. 10:412–424
doi:10.2136/vzj2010.0079
Received 11 June 2010.
Published online 20 Jan. 2011.

Three-Dimensional Electrical Resistivity Tomography to Monitor Root Zone Water Dynamics

Knowledge of soil moisture dynamics and its spatial variability is essential to improve our understanding of root water uptake and soil moisture redistribution at the local scale and the field scale. We investigated the potential and limitations of electrical resistivity tomography (ERT) to measure three-dimensional soil moisture changes and variability in a large, undisturbed, cropped soil column and examined the interactions between soil and root system. Our analysis sustained the value of ERT as a tool to monitor and quantify water contents and water content changes in the soil, as long as the root biomass does not influence the observed resistivity. This is shown using a global water mass balance and a local validation using time domain reflectometry (TDR) probes. The observed soil moisture variability was rather high compared to values reported in the literature for bare soil. The measured water depletion rate, being the result of combined effects of root water uptake and soil water redistribution, was compared with the evaporative demand and root length densities. We observed a gradual downward movement of the maximum water depletion rate combined with periods of redistribution when there was less transpiration. Finally, the maximum root length density was observed at –70 cm depth, pointing out that root architecture can strongly depend on soil characteristics and states.

Abbreviations: DOY, day of year; DR, depletion rate; EC_b, bulk soil electrical conductivity; ERT, electrical resistivity tomography; ET, evapotranspiration; GPR, ground penetrating radar; nDR, normalized mean weekly water depletion rates; RLD, root length density; RWU, root water uptake; TDR, time domain reflectometry; WC, water content; W-S, Waxman and Smits (1968) [model].

Accurate knowledge of the processes governing soil moisture variability and water redistribution in the soil–plant continuum is necessary for agricultural water management and predictions of the fate of agrochemicals. The amount of water plants can take up and transpire depends on soil water availability and the distribution of roots in the soil. However, controversy still remains about the main factor(s) controlling root water uptake, especially for a nonuniform soil moisture distribution and intermediately wet soil (Green et al., 2006). Due to nonlinear dependencies on water content, upscaling of root water uptake and evapotranspiration requires knowledge of the spatial statistics of local water contents. During the past decades, many studies have focused on measuring and understanding soil moisture variability at the field-scale and its interaction with root water uptake (RWU) (Katul et al., 1997; Coelho and Or, 1999; Green and Clothier, 1999; Vrugt et al., 2001b; Teuling and Troch, 2005; Vereecken et al., 2008). However, the conclusions of these studies differ with respect to the mechanisms controlling spatial variability of soil moisture. Both soil properties and root water uptake processes may create or reduce spatial variability of soil moisture (Teuling and Troch, 2005). As Coelho and Or (1999) stated, actual water uptake patterns in the field reflect a complex interplay between the root system and other soil factors such as water, nutrient and aeration status of the root zone.

Until now, a large number of the studies dealing with the interplay of plant roots and soil moisture at the large column or field scale involved either destructive measurements of water contents such as soil cores (e.g., Sharp and Davies, 1985) or a grid of in situ measurement techniques including TDR (e.g., Katul et al., 1997; Musters and Bouten, 1999; Musters and Bouten, 2000; Teuling and Troch, 2005) and neutron probes (e.g., Vrugt et al., 2001a; Hupet et al., 2002a; Koumanov et al., 2006). Destructive measurements do not provide information on the temporal dynamics of the soil moisture, and in situ measurement techniques have a good temporal resolution but limited spatial extent and coverage.

In addition to highly resolved soil moisture measurements in space and time, studying the interaction between soil moisture and the root system also requires monitoring of root

growth and densities. Root densities were frequently measured destructively using soil cores (e.g., Sharp and Davies, 1985; Katul et al., 1997; Coelho and Or, 1999; Green and Clothier, 1999). Minirhizotrons offer the possibility to observe the development of the root system in a nondestructive, yet invasive, way in large soil columns (e.g., lysimeters). Minirhizotron images give spatial and temporal information on root characteristics in the soil (e.g., Heeraman et al., 1993; Merrill and Upchurch, 1994; Dubach and Ruselle, 1995; Hendrick and Pregitzer, 1996; Johnson et al., 2001; Bernier and Robitaille, 2004). Nonetheless, the observed volume of the root zone is very small, and obtaining high temporal resolution is hampered by the high work load of the method.

Electrical resistivity tomography allows us to monitor the volumetric soil water content (WC) with a higher temporal and spatial resolution as compared to conventional methods by measuring the bulk soil electrical conductivity (EC_b), which is related to the WC. It has an advantage over ground penetrating radar (GPR) because GPR performance decreases in electrically conductive media such as fine-textured soils. Electrical resistivity tomography has mainly been used to monitor drainage and infiltration processes (Stubben and LaBrecque, 1998; Glass et al., 2002; LaBrecque et al., 2002; Zhou et al., 2002; Descloitres et al., 2003; French and Binley, 2004; Amidu and Dunbar, 2007) and to image and characterize solute transport in bare soils (Binley et al., 1996a,b; Henry-Poulter, 1996; Koestel et al., 2008; Koestel et al., 2009b). Besson et al. (2004) and Séger et al. (2009) used the technique to characterize the structural heterogeneity of the soil and showed that big structural entities, such as a compacted plow pan, can be recognized. Electrical resistivity tomography has been applied at a range of scales, from the lab (e.g., Olsen et al., 1999; Werban et al., 2008), to the lysimeter (e.g., Binley et al., 1996a; French et al., 2002; Koestel et al., 2009a; Garré et al., 2010), and up to the field scale (e.g., Daily and Ramirez, 1995; Slater et al., 1997; Daily and Ramirez, 2000; LaBrecque et al., 2002; Oberdörster et al., 2010). Only a few studies have used ERT to estimate root water uptake or root densities. Michot et al. (2003) monitored soil moisture changes in an unsaturated, irrigated soil under corn (*Zea mays* L.) using surface ERT. They showed that an in situ calibration was needed to convert EC_b, derived from ERT to WC, since the relationship depended on the volume of soil. Similar results were obtained by Srayeddin and Doussan (2009), who also used ERT to measure RWU under maize and sorghum [*Sorghum bicolor* (L.) Moench] in the field. Additionally, they concluded that the sensitivity–resolution of the technique should be optimized in field settings to improve the quantitative estimation over the whole rooted zone. This problem has been addressed in several studies (Friedel, 2003; Furman et al., 2004; Stummer et al., 2004; Gharibi and Bentley, 2005; Maillet et al., 2005; Singha and Gorelick, 2006; Singha and Moysey, 2006). However, general conclusions about an optimal ERT setup cannot be drawn since sensitivity and resolution of ERT do not only depend on the electrode configuration, but also on the heterogeneity of the studied system, its overall conductivity, and the magnitude of changes during the measurement period. In addition, several studies reported on the effects of the presence of roots on the EC_b (Al Hagrey, 2007; Werban et al., 2008; Zenone et al., 2008; Amato et al., 2009), but the results were equivocal. It is expected that young, nonsuberized roots will increase the EC_b, while older, suberized root segments may decrease the conductivity. In addition, EC_b might be affected by water filling or depletion of the possibly changing void space between the root and the soil matrix.

We used ERT to measure three-dimensional soil moisture changes in a system as close as possible to a cropped field, that is, in a large lysimeter, with a growing crop, undisturbed soil horizons, and other elements of heterogeneity, such as earthworm holes and fissures, present in the monolith. The aim of this study was to (i) investigate the potential and limitations of ERT to monitor three-dimensional soil moisture changes in a natural, cropped soil over a range of soil moistures using an in situ calibration of the pedophysical relationship; (ii) validate the ERT measurements in a global way, using a total water mass balance, and in a local way, using measurements of local water contents with TDR; (iii) examine the influence of root water uptake on soil moisture variability and soil moisture changes with time; and (iv) observe root growth noninvasively using a minirhizotron and link it to the observed soil moisture changes.

Material and Methods

Experimental Design of the Barley Experiment

An undisturbed soil monolith was sampled using a large PVC column with a height of 150 cm and an inner diameter of 116 cm. The monolith was taken from intensively used arable land near Merzenhausen, Germany. The soil that developed in the Loess parent material was classified as an orthic Luvisol (FAO classification system). Four soil horizons were identified: A_p (0–40 cm), B_t (41–70 cm), B_{v1} (71–100 cm), and B_{v2} (>100cm). More information on this soil can be found in Garré et al. (2010). The PVC column was driven into the soil gently using the hydraulic shovel of an excavator. To reduce friction, the soil around the column was excavated and the bottom of the PVC column was sharpened. When the column was completely filled with soil, a steel plate was driven horizontally under the monolith to isolate the monolith. The monolith was transported to the lysimeter facility of the Forschungszentrum Jülich where it was placed on a scale (Bizerba, Balingen, Germany). The upper boundary of the lysimeter was aligned with the soil surface in the lysimeter facility and the column was covered from rainfall by a greenhouse construction. The bottom boundary of the lysimeter was kept at −50 hPa by a polyamid-membrane suction plate (ecoTech GmbH, Bonn, Germany) and a vacuum pump (UMS, Munich, Germany). We equipped the lysimeter with a vertical transect of four horizontally installed minirhizotron tubes at depths of −19.5, −44.5, −69.5 and −119.5 cm. The tubes are made of plexiglass, are 60 cm

long, and have a diameter of 5.72 cm. A BTC2 video microscope (Bartz Technology Corporation, Carpinteria, CA) was used to monitor root length density (RLD) and root growth on the outer walls of the tubes. Two hundred twelve electrodes were inserted at the side of the column extending 1.5 cm into the soil. The electrodes at the side of the column were arranged in six horizontal rings of 32 equidistantly distributed electrodes. Between these circles we added four vertical transects of five electrodes (Fig. 1). Details about the electrode arrangement are documented in Koestel et al. (2008) and Garré et al. (2010). The electrodes were connected with relay boxes to a six channel RESECS prototype (GeoServe, Kiel, Germany) to conduct ERT measurements.

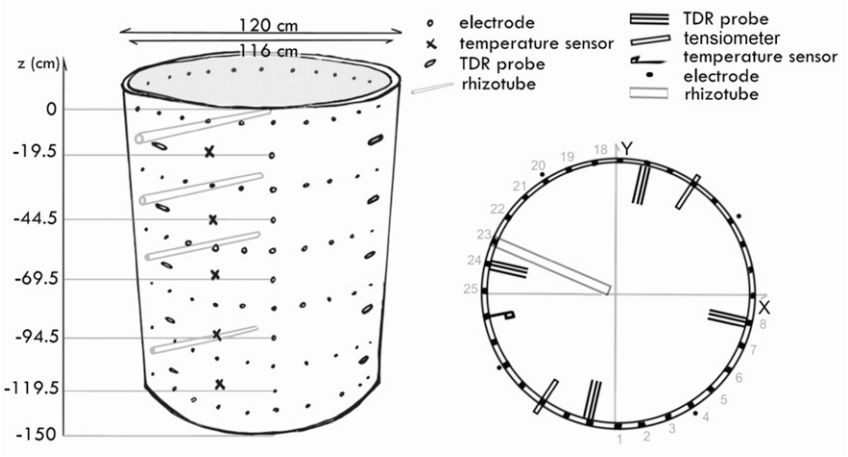

Fig. 1. (left) Lysimeter with equipment and (right) horizontal cross-section of the soil column. The four black dots at the side of the horizontal cross-section indicate the vertical transects with additional electrodes.

To measure water content and bulk electrical conductivity, we inserted 20 horizontal TDR probes in four opposite vertical transects at depths of −19.5, −44.5, −69.5, −94.5 and −119.5 cm. We used a three-rod design (Heimovaara, 1993) with a rod length of 19 cm, a rod spacing of 2.6 cm, and a rod spacing/diameter ratio of 13:2. A TDR100 system, SDMX50 multiplexers, and CR10X data logger (Campbell Scientific, Logan, UT) were used to conduct and log the TDR measurements at 1-h intervals. The TDR probes could not be distinguished from the soil matrix in the ERT measurements. This was also observed by Koestel et al. (2008). In addition to the TDR probes, six platinum resistance thermometers (PT100) were installed, five at the same depths as the TDR probes and one inserted at the bottom of the lysimeter. A DL2e data logger (Delta-T Devices Ltd., Cambridge, UK) registered the tensiometer and PT100 sensor data. A Cond i325 conductivity meter (WTW, Weilheim, Germany) measured the electrical conductivity of the effluent. Figure 1 gives an overview of the complete experimental set-up.

At the start of the experiment, the volumetric water content in the bare column measured with TDR varied with depth between 0.30 and 0.45. After the summer barley (*Hordeum vulgare* L.) was sown in parallel lines approximately 20 cm apart on Day of Year (DOY) 132, the soil did not receive any additional water until DOY 209. The first day of the experiment was thus DOY 132. Crop senescence started at Day 60, which corresponds to DOY 192.

Electrical Resistivity Tomography

We used a three-dimensional inversion of the ERT data to image changes in soil EC_b. A "skip one" dipole–dipole scheme was used, as described in Slater and Sandberg (2000). To assess the data quality, one-half of the measurements were reciprocal measurements (LaBrecque et al., 1996). A finite element method was used to solve the Poisson equation, which is the forward problem:

$$\nabla\cdot(\mathrm{EC_b}\nabla\varphi)-\nabla\cdot j_s=0 \qquad [1]$$

where EC_b is the bulk soil electrical conductivity (S m^{-1}), φ the electric potential (V), and j_s the source current density (A m^{-2}). No-flow boundary conditions were applied on all boundaries.

The inversion was performed using an error-weighted, smoothness constrained Occam type algorithm. This means that the smoothest model distribution that fits the data to a specified error level was searched for. Given a set of N measurements of four-electrode resistance (R_i, i = 1,2,...,N), minimization of the objective function, Ψ, given by

$$\Psi=\left\|\mathbf{W}_\varepsilon\left[\mathbf{d}-f(\mathbf{m})\right]\right\|_2^2+\lambda\left\|\mathbf{W}_s(\mathbf{m}-\mathbf{m_0})\right\|_2^2 \qquad [2]$$

produces an image of M voxel electrical resistivities ρ_j (j = 1,2,...,M), where $m_j=\log(\rho_j)$, $\mathbf{d}$ is the data vector, $f(m)$ is the forward model that relates the model m to the measured apparent resistivities, $\mathbf{W}_s$ is a smoothness operator, $\mathbf{W}_\varepsilon$ is an error weighting matrix, and λ is a regularization parameter that determines the amount of smoothing imposed on m during the inversion. More information on the implementation of the objective function is given in Garré et al. (2010). An unstructured tetrahedral mesh with grid refinement close to the electrodes was used to calculate the electric potential. After the inversion, the data where interpolated on a structured wedge mesh with voxel height of 6.95 cm to represent the variability of the electrical conductivity. For further details on the inversion we refer to Kemna (2000) and Guenther et al. (2006).

The data error (ε_i) was calculated as in Koestel et al. (2009a). It was assumed that the data error can be approximated using a Gaussian error model that comprises an absolute resistance error component, $p(\Omega)$, and a relative resistance error component, q. These two components are then used in the inversion algorithm to calculate the error (ε_i) of each single data point d_i as follows:

$$\varepsilon_i = \frac{p}{R_i} + q \quad [3]$$

The approach considers the error model being spatially and temporally constant, to reduce the degrees of freedom in the error estimation. To keep the inversion equal for all timeframes, a constant p and q were used for the inversion and set to the maximum p and q of the whole time series.

Conversion of Bulk Electrical Conductivity to Water Content

Topp's equation (Topp, 1980) was used to relate the volumetric water content of the soil [WC(TDR)] to the composite dielectric constant (ξ_c) measured by TDR:

$$\mathrm{WC} = -5.3\times10^{-2} + (2.92\times10^{-2})\xi_c - (5.5\times10^{-4})\xi_c^2 + (4.3\times10^{-6})\xi_c^3 \quad [4]$$

This calibration curve proved to be successful in soils that do not contain substantial amounts of bound water (Robinson et al., 2003).

There are various existing pedophysical models published in the literature which relate the measured bulk electrical resistivity to the factors influencing this resistivity—surface conductivity of the soil matrix, pore water conductivity, porosity of the soil, temperature and water content (e.g., Archie, 1942; Waxman and Smits, 1968; Revil et al., 1998). Waxman and Smits (1968) (W-S) developed such a pedoelectrical model based on Archie's law (Archie, 1942) for the use in geological applications. Recently, it has been successfully applied by several authors for quantifying transport processes in the unsaturated zone using ERT (e.g., Koestel et al., 2009a,b; Garré et al., 2010). For this study, we used a simplified empirical equation closely related to the W-S model:

$$\mathrm{EC_b} = a\mathrm{WC}^n + b \quad [5]$$

where a (S m^{-1}), b (S m^{-1}), and n are fitting parameters. In this equation, the surface EC is not affected by the water content or solution EC. The parameters in the simplified W-S function can thus still be interpreted in a physical manner: a is affected by the pore water conductivity and b by the soil surface conductivity, both in combination with the porosity (± constant for a soil horizon, but can be different between horizons). There is no consensus on the physical meaning of n for the full W-S model, but it may be related to, for example, the pore connectivity.

We derived in situ pedophysical models for each soil horizon based on the simplified W-S model using $\mathrm{EC_b}$(ERT)–WC(TDR) couples at the TDR probe locations during the experiment in the lysimeter. Here, $\mathrm{EC_b}$(ERT) is the mean of inverted bulk electrical conductivities in the measurement volume of a TDR probe. This resulted in four $\mathrm{EC_b}$–WC couples for each measurement time and each of the five depths with TDR probes. We grouped the $\mathrm{EC_b}$–WC couples in four categories belonging to four different pedological horizons as observed in the field and fitted the simplified W-S model to the data in each of the four horizons:

$$\mathrm{WC(ERT)} = \left\{\frac{[\mathrm{EC_b(ERT)} - b]}{a}\right\}^{1/n} \quad [6]$$

where a (S m^{-1}), b (S m^{-1}), and n are fitting parameters. At −44.5 one of the four TDR probes and at −119.5 two TDR probes were malfunctioning and discarded. By assuming one specific pedophysical relationship for a soil horizon, we discard some of the variability present in the volume.

Monitoring Root Length Density

To derive the RLD, images were taken once a week along the horizontal rhizotubes at 10 different locations in each tube. One image encompasses a soil window of approximately 1.5 by 2.2 cm^2, and a viewing depth of 0.1 cm is assumed (Taylor et al., 1970; Sanders and Brown, 1978; Itoh, 1985; Steele et al., 1997). An example of successive images in Tube 2 is given in Fig. 2. The images were analyzed using the open source software RootFly (Wells and Birchfield, 2009). We used the software to register the length, diameter, and color of the roots. From the root length in each image, the RLD can be estimated as the length of the roots per unit volume of the sample, being 1.5 by 2.2 by 0.1 cm^3. The root length density at a certain depth was then the mean RLD of all the locations at that depth.

Total Mass Balance Calculation

To understand the interaction of a crop and the soil moisture status, we estimated the different fluxes in and out of the soil. The weight (m, g) of the lysimeter was logged with an accuracy of 200 g. As

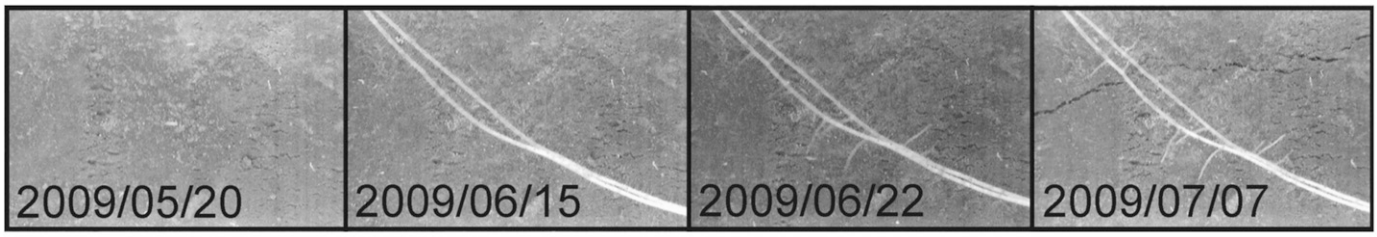

Fig. 2. Four consecutive minirhizotron images at 38 cm from the lysimeter edge in Tube 2.

no water was added to the soil during the experiment, changes in weight are equal to the sum of evapotranspiration (ET, m d^{-1}) and drainage (D, m d^{-1}). We used a glass vessel under suction to collect the effluent. Each time the effluent volume in the vessel reached 500 mL, the vessel was emptied and the time was logged. From the logged times, and the known drainage volume, the drainage rate D was calculated.

The evaporation rate was estimated using the evaporation rate from a 5.8-cm-deep water pan with a surface of 45 by 35 cm^2. The evaporation loss from the water pan was related to the reference evapotranspiration (ET_0) and the potential crop evapotranspiration (ET_c) by applying empirical coefficients (see Allen et al. [1998] for the exact equations). As such, ET_c represents the sum of the crop transpiration (T) and the soil surface evaporation (E). In this experiment, E is supposed to be very small or even equal to zero, since the soil surface was very dry and the crop covered a large part of the surface. For each time step, we calculated the water loss from the difference between the initial water content and the water content at that time in the whole lysimeter volume. The water loss monitored with ERT was then compared with the weight loss of the lysimeter. This comparison allowed us to evaluate the performance of the ERT measurements and the pedophysical relationship to establish a water balance over time. The total correspondence of both measurements was tested with the root mean squared error (RMSE).

Results

In situ Calibration of Electrical Resistivity Tomography Measurements

The EC_b–WC relationship for each of the four horizons in the lysimeter is shown in Fig. 3. Table 1 shows the parameters of the simplified W-S model and the RMSEs of the optimized functions. The optimization was done by the minimization of a simple objective function (the RMSE) using the Nelder–Mead simplex method, an unconstrained nonlinear optimization algorithm. The pedophysical relations vary considerably between the different soil horizons. This was expected since the surface conductivity is influenced by the clay content, which is different across horizon, just like the porosity. In general, the simplified W-S model describes the data well for all horizons but the A_p. The course of measured EC_b–WC data in the A_p is more curved than the W-S fit. The rather bad fit in this horizon is probably due to the data at the end of the growing season. Starting from Day 63 of the experiment (DOY 195), the EC_b in the A_p horizon apparently started to increase with decreasing moisture content, which leads to traces of EC_b–WC points (marked with two black arrows in Fig. 3) deviating from the expected relation. In the B_t horizon, more specifically the TDR probes at the −44.5-cm depth, a part of the general course of the EC_b–WC couples cannot be described entirely by the simplified W-S model (white arrow in Fig. 3). Also in B_{v1} some deviations are visible, but these are less systematic than

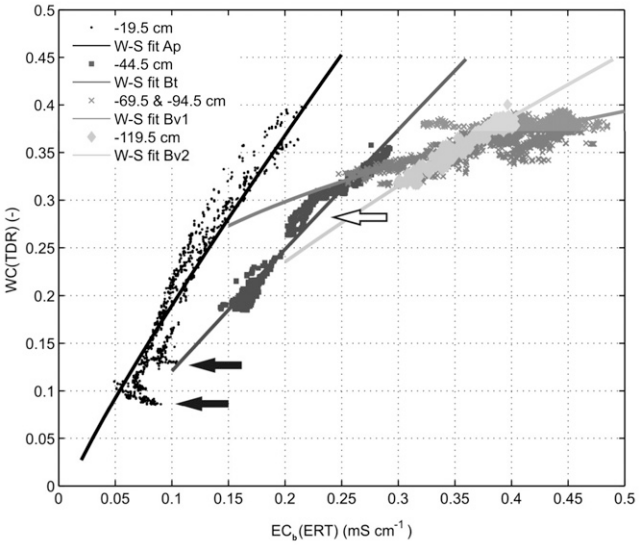

Fig. 3. Bulk soil electrical conductivity by electrical resistivity tomography and water content by time domain reflectometry [EC_b(ERT)–WC(TDR)] couples and simplified Waxman and Smits (1968) (W-S) fits to these couples for four soil horizons. The black arrows indicate misfits starting in the 10th week of the experiment. The white arrow indicates a misfit in the B_t horizon.

Table 1. Parameters for the simplified Waxman and Smits (1968) model for each of the four horizons.

Horizon	*a*	*b*	*n*	RMSE
	mS cm^{-1}			
A_p (greater than −40 cm)	0.5861	0.00999991	1.1271	0.03
B_t (−40 to −70 cm)	0.8037	0.00999531	1.0356	0.01
B_{v1} (−70 to −100 cm)	12.0495	0.00999998	3.4314	0.01
B_{v2} (less than −100 cm)	1.5033	0.00166441	1.3996	0.005

in the former horizons. These deviations from the fitted function can inflict small errors in the estimated water contents. As mentioned in the introduction, there is experimental evidence that the root biomass can alter the EC_b in both directions depending on the plant and root characteristics (Al Hagrey, 2007; Werban et al., 2008; Zenone et al., 2008; Amato et al., 2009). For herbaceous plants, an increase of conductivity was reported. Since the observed anomalies in the general trend occur in the two upper TDR probes, they may be caused by the presence of a critical amount of roots in the measurement volume in combination with a relatively dry soil. The increased EC_b for the same water content at the end of the experiment (in the dry range) might be caused by an alteration of the roots as the experiment was near to the end of the growing season. Using the minirhizotron images, we could observe that the roots were shrinking after Day 60 (DOY 192) at depths of −44.5 and −69.5 cm. This change of root structure as well as a change of physical contact between root and soil might explain the changing pedophysical relationship. However, at −69.5 cm there is not a clear change of the pedophysical relationship when the roots start

shrinking, maybe because the soil is not that dry yet. In addition, as the soil dries out the electrode contact might reduce so that the ERT measurement error and thus the noise on the ERT-derived WC becomes larger for lower EC_b. This can also add deviations to the data in the dryer range.

Water Content Distributions and Profiles in the Lysimeter

Figure 4 shows three-dimensional water content distributions at three different days that were derived from ERT measurements. The irregular and nonhorizontal surfaces of constant water content demonstrate the heterogeneity of the drying process in the lysimeter. To obtain these three-dimensional images of water content, the ERT-derived bulk electrical conductivity distributions were translated into water contents using the pedophysical relations.

Figure 5 shows the bulk electrical conductivity in a vertical section of the soil column after 38 d. The black horizontal lines represent the depths of the horizon boundaries as they were observed in the field. Each of the horizons is characterized by a different pedophysical relationship (Fig. 3). This differentiation adds structures to the moisture distribution in the lysimeter, which are not visible in the inverted bulk conductivity data. Figure 6 depicts profiles of horizontally averaged bulk electrical conductivities and water contents for different times, as well as the standard deviation of the ERT-derived water contents. Unlike the EC_b profiles, the ERT-derived water content profiles have important discontinuities at the soil horizon boundaries. The depths of these boundaries were not derived from ERT measurements but were based on observations in a nearby soil profile pit in the field. The shape of the boundary was approximated by a horizontal flat surface, since the resolution of ERT is not high enough to derive the real, probably slightly undulated boundary from the resistivity measurements. The abrupt changes in soil moisture were a consequence of the assumption that pedophysical relation changed abruptly across the soil horizon boundary. Nevertheless, abrupt changes in water content may occur across boundaries of soil layers with different hydraulic properties. A validation of the exact location of the soil horizon boundaries, the shape of the boundary, and the gradient of the pedophysical relations across this boundary requires additional information. This information could be obtained potentially from other geophysical measurement techniques, such as georadar, which are sensitive to abrupt changes in water content or from process monitoring, such as transport experiments. Finally, it is of importance to notice that root development may also be affected by soil textural discontinuities leading to an additional uncertainty in the estimation of the soil moisture content at these boundaries.

Local Validation of the Soil Moisture Distribution

To compare the results of ERT and TDR measurements, we averaged the ERT voxels in the TDR measurement volume. Figure 7a shows the variability of the WC measured with the TDR probes against the variability of the WC from ERT in the measurement volume of the TDR probes for four depths. Soil moisture content measurements at a depth of −119.5 cm were not included because two of four TDR probes did not function properly. The variability measured with ERT and TDR are in the same range. This indicates that applying one W-S model for a soil layer and using the smoothness constraint in the ERT inversion neither added nor removed variability artificially. The hatched area marks all standard deviations lying below the RMSE of the fitted pedophysical relationship for the horizon under consideration. It becomes clear that only for the TDR probes that were closest to the soil surface the variability of the measured WC is high enough to validate the variability of the ERT measurements. However, the RMSE is a crude measure to evaluate a fit, and bad correspondence in a small period of time can have a large influence on the overall RMSE of

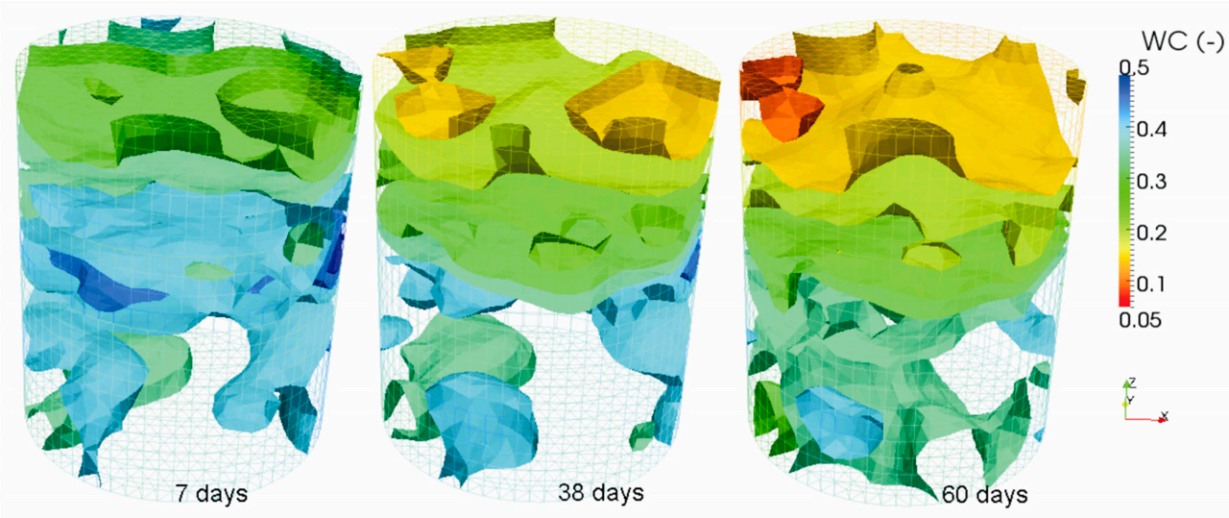

Fig. 4. Three-dimensional volumetric water content in the lysimeter after 7, 38, and 60 d. The surfaces are isosurfaces of equal water content. The distance between two isosurfaces is 0.05.

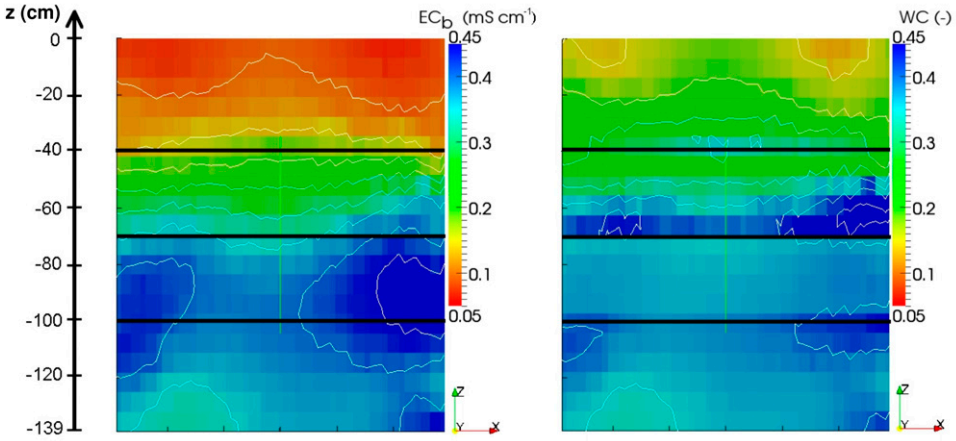

Fig. 5. (right) Water content (WC) in a vertical section through the lysimeter estimated from ERT data 38 d after sowing. (left) Bulk electrical conductivity (EC_b, mS cm^{-1}) in a vertical section through the lysimeter 38 d after sowing. In both plots contour lines are displayed for each interval of 0.05 for WC and 0.05 mS cm^{-1} for EC_b. The soil horizons boundaries are indicated with black lines.

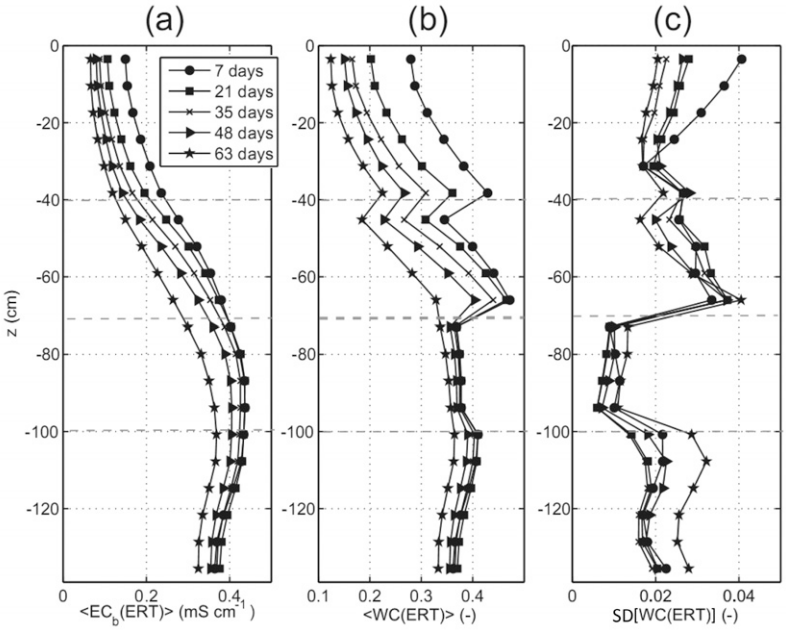

Fig. 6. (a) Mean bulk electrical conductivity (<EC_b>) and (b) mean (<WC>) and (c) standard deviation of the water content [SD(WC)] from electrical resistivity tomography measurements for all voxel layers in the lysimeter for $t = 7$, 21, 35, 48, and 63 d after sowing. The horizontal dotted lines delineate the soil horizons.

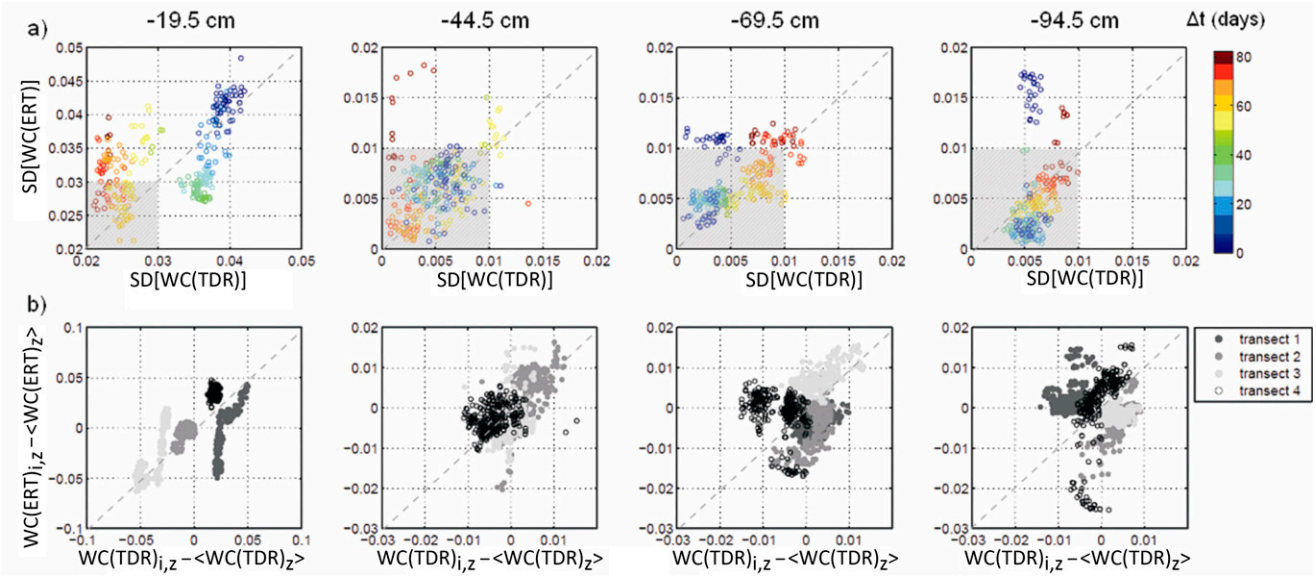

Fig. 7. (a) Scatter plot of the standard deviation of the water content obtained by time domain reflectometry (TDR) and the one estimated by electrical resistivity tomography (ERT). (b) The difference of the water content (WC) and mean WC for a depth for ERT against the same for TDR. The conductivities used to estimate WC(ERT) were the average of the voxels lying within the TDR measurement volume and therefore represent the mean WC [<WC(ERT)>] for that measurement volume.

a fit. Therefore, this is a very strict criterion to evaluate the measured variabilities. In Fig. 7b, the deviations of WC(TDR) and WC(ERT) from the mean WC(TDR) [<WC(TDR)>] and the mean WC(ERT) [<WC(ERT)>] at a certain depth are plotted against each other. A clustering of these deviations around the 1:1 line indicates that not only the total variability but also the patterns of the soil moisture variability are represented well by ERT. This can be represented quantitatively by an adjusted coefficient of determination (R^2), which is a measure for the fraction of the spatial variability of the TDR measurements explained by the WC derived from ERT measurements:

$$R^2 = 1 - \frac{\sum_{i,j}\left\{\left[\mathrm{WC(ERT)}_{i,j} - \left\langle \mathrm{WC(ERT)}_j \right\rangle\right] - \left[\mathrm{WC(TDR)}_{i,j} - \left\langle \mathrm{WC(TDR)}_j \right\rangle\right]\right\}^2}{\sum_{i,j}\left[\mathrm{WC(TDR)}_{i,j} - \left\langle \mathrm{WC(TDR)}_j \right\rangle\right]^2} \quad [7]$$

Unlike the classic coefficient of determination, the adjusted R^2 can be negative, and will always be less than or equal to R^2. The R^2 values for the depths of −19.5, −44.5, −69.5, and −94.5 cm are 0.37, 0.29, −0.34, and −0.97. The first two depths have an acceptable R^2. The variability and patterns of ERT and TDR correspond, and the variability is high enough to be able to distinguish patterns from measurement and fitting noise. Conversely, the coefficient of determination at depths of −69.5 and −94.5 cm is negative. Additionally, the WC variability measured with TDR in these depths (<0.01) was not high enough to be able to show the difference between measurement noise and real patterns. This can explain the R^2 values. However, since we showed that ERT is capable of capturing the level of variability and the patterns of WC well in the top horizon, where the variability is higher, we assume that this will also be the case in the lower horizons when the soil dries out and the variability increases.

Global Water Mass Balance Analysis

An additional, indirect way to validate the water content profiles that were derived from ERT is to compare the total water loss obtained by weighing with the sum of the water loss in each voxel of the ERT mesh (Fig. 8). The water loss from weight and ERT data agree very well. The RMSE between total water loss obtained by weight and the loss derived by ERT is 0.0032. Notice that between t = 42 and 48 d no data were available due to technical problems with the data loggers. There are some small deviations visible between ERT and weight measurements. Between Day 20 and 30, for example, the total water content estimated with ERT decreased more rapidly than the one from the lysimeter weight. This is probably due to deviations between the fitted W-S model in the A_p horizon and the data. Since we observed drainage only during the first 14 d of the experiment, the weight loss after Day 14 is entirely due to evapotranspiration. During the first 14 d, the bottom flux decreased from 0.13 cm d^{-1} the first day, to>0.05 cm d^{-1} already the second day, with no drainage at Day 15. The drainage was therefore negligible when compared with the total weight loss already after a few days.

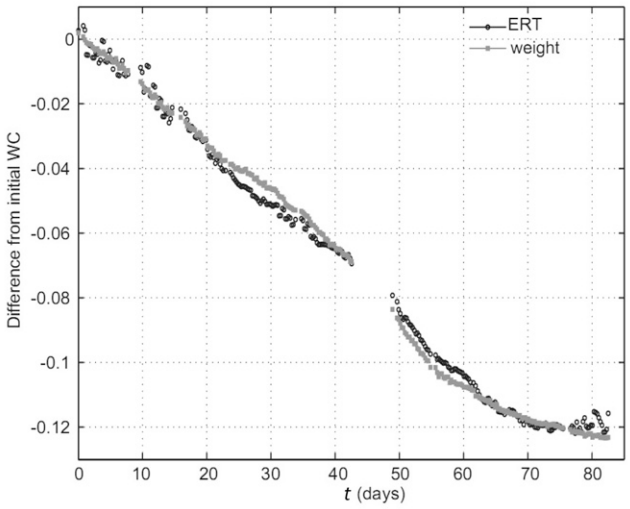

Fig. 8. Mass balance of the lysimeter during the whole experiment.

Evolution of Soil Moisture Variability at the Voxel Scale

The evolution of water content with time in two planes intersecting the column at −20 and −80 cm, respectively, are depicted in Fig. 9. In general, the observed WC variability is much lower in the horizontal than in the vertical direction. The soil moisture pattern, i.e., the location of the driest and wettest regions in the horizontal cross-section, at −20 cm changed during the course of the experiment. The observed patterns could not be linked visibly to the barley rows. Also at a depth of −80 cm, the soil moisture patterns changed during the experiment, but the variation of soil moisture in time and space was smaller than at a depth of −20 cm, as we already noticed looking at the TDR measurements. Figure 10 shows the relation between mean water content for five different voxel layers of the soil column and the standard deviation of the WC at the voxel scale (h_{voxel} = 6.95 cm) for the measurement period. At the first and second depth, the variability is the highest when reaching an intermediate moisture content of approximately 0.3. For lower mean values the standard deviation decreases with decreasing mean WC. At the end of the experiment, which corresponds to low mean average water content values, the variability of the water contents seems to increase again. As stated before, this might be an artifact caused by root effects on the soil electrical conductivity. In the lower voxel layers, the variability was still increasing at the end of the experiment and reached a higher level than the maximum variability in the upper voxel layers. Figure 6 shows that there are not only important gradients in the WC across horizon boundaries, but also gradients in variability. The fact that this variability is observed already at Day 0 indicates that at least a part of the variability must be linked to the hydraulic properties of the different horizons, as Vereecken et al. (2007)

indicated. The same authors showed that the relationship between soil moisture variability and mean moisture content for a bare soil is controlled by soil hydraulic properties, their statistical moments and their spatial correlation. Because roots will develop differently in each horizon depending on soil hardness, soil water, and nutrients availability (Bengough et al., 2006), and since root uptake will also differ following soil and root hydraulic properties, this effect may be accentuated or decreased when soil is cropped. For a bare silty loam, Vereecken et al. (2007) predicted a maximum standard deviation of 0.05. This soil type is comparable to the silty orthic Luvisol in this study, but the maximum standard deviation of our data set is higher. This discrepancy could be caused by spatially variable root water uptake and data noise.

Water Depletion Rate

Water depletion rates (DR, d^{-1}) in a horizontal layer of voxels were calculated from the change in average WC in the layer over a given time interval. The weekly rates were computed by moving a time window of a week day per day and taking the average over a week (moving average):

$$DR_j = \frac{\sum_{i=1}^{7}\left[\frac{\left(WC_{i+j} - WC_{i+j-7}\right)}{\left(t_{i+j} - t_{i+j-7}\right)}\right]}{7} \quad [8]$$

where i represents the day of the week (1–7) and j = [7, 14, 21,...,77] days. The total water depletion rate in the lysimeter (DR_{total}, m d^{-1}) was obtained from integration of the average water depletion rates in the horizontal voxel layers over the lysimeter depth (Fig. 11a). The water depletion rates in the voxel layers were then normalized by DR_{total}. These normalized mean weekly water depletion rates (nDR, m^{-1}) are displayed in Fig. 11b as a function of time. Negative nDRs imply that the water content has increased over time at a certain depth. The line plot on top of the nDR evolution shows the resulting DR_{total} calculated from the ERT data as well as from the weight data to validate the ERT-derived DRs.

The observed mean weekly DR_{total} varies between 0.1 and 0.4 cm d^{-1}. Due to the wet soil conditions at the start of the experiment,

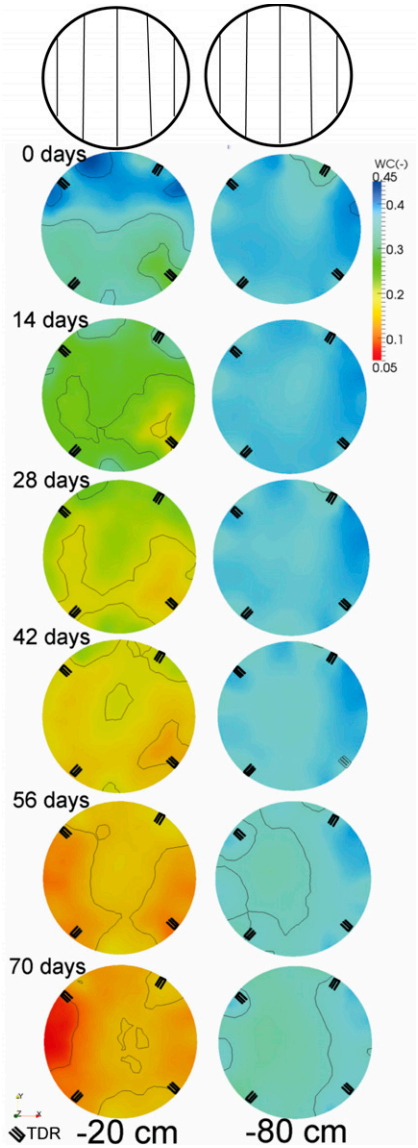

Fig. 9. Horizontal section through the three-dimensional water content (WC) distribution in the lysimeter at depths −20 and −80 cm. The orientation of the barley rows is shown at the top of the image. The contours of [0.05,0.45] with steps of 0.05 are indicated with black lines. Please note that the time domain reflectometry (TDR) symbols show the location of the vertical TDR transects in a horizontal section of the soil column. There are no TDR probes in the depicted planes (at depths of −20 or −80 cm).

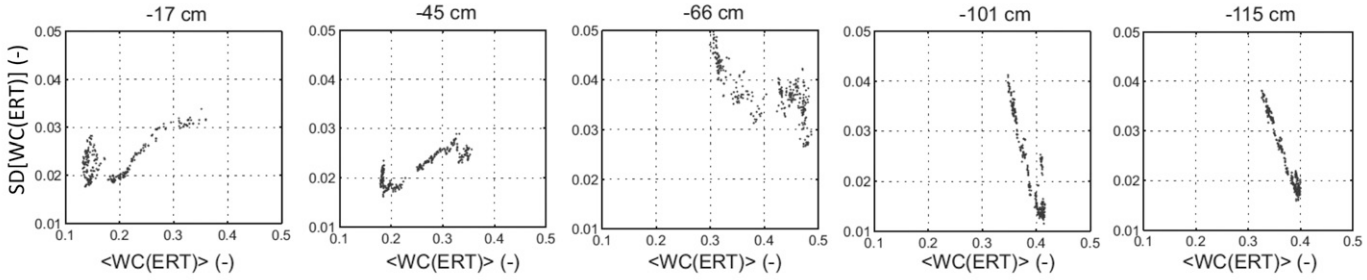

Fig. 10. Standard deviation of the water content [SD(WC)] in voxel layers at −17, −45, −66, −100, and −115 cm as a function of the mean of the water content at the same depths.

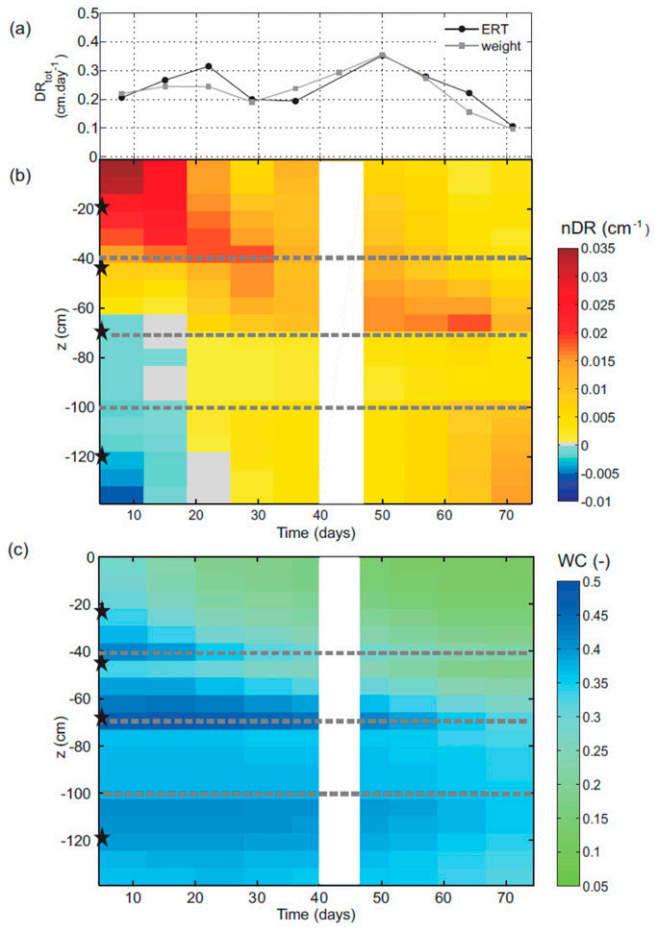

Fig. 11. (a) Total weekly water depletion rate (DR_{tot}) estimated by electrical resistivity tomography (ERT) and weight measurements; (b) normalized local water depletion rates (nDR) as a function of depth and time; (c) volumetric water content (WC) measured with ERT as a function of depth and time. The black stars indicate the rhizotube locations. The gray dashed line indicates horizon interfaces.

there was a considerable water redistribution and internal drainage at the beginning of the experiment. This led to an increase in water content in the bottom half of the lysimeter. During the first 20 d of the experiment, the front of maximum nDR stayed in the upper soil horizon and moved down gradually afterward. From Day 19 until Day 32, the maximum nDR is at the 0.4-m depth, and a decrease of nDR can be observed at the top of the column. The decrease in nDR in the top soil may be the effect of a lower ET during this period in combination with water redistribution toward the top soil layer. The nDR increased again at the top of the lysimeter together with a slightly higher ET from Day 35 until Day 45. From Day 45 until Day 55, the ET is considerably larger than in the previous periods, but the water in the top soil is depleted, so the maximum nDR moves downward. This could indicate that stress was occurring in a part of the root zone, causing the plant to adjust its rooted volume, or the effectiveness of already existing roots. Potential ET rates were calculated from measured water pan evaporation rates (Allen et al., 1998). At the beginning of the experiment, the DR_{total} values were higher than the calculated potential ET rates. This was due to an underestimation of the bare soil evaporation in the Allen et al. (1998) procedure. From Day 25 until 58, the potential ET rates corresponded well with DR_{total}. The decrease in ET rate between Day 50 and Day 58 cannot be linked with water stress but is rather due to different meteorological conditions. Therefore, downward movement of the DR_{total} from Day 50 due to water shortage in the top soil probably did not lead to a water stress at the plant level. From Day 60, the measured DR_{total} was smaller than the calculated potential evaporation of a full-grown barley crop. After Day 60, crop senescence started, and the transpiration rate reduced. The senescence of the barley in the lysimeter was not caused by the soil water regime in the lysimeter and cannot be linked to a water stress of the plants, since the barley in the field surrounding the lysimeters entered senescence around the same time.

Significant water loss below 70 cm in the B_v horizons occurred only after 60 d. Before the nDR front moved into the Bv horizon, it seemed to be blocked at the upper boundary of the Bv horizon. In the field we observed that these horizons were harder to penetrate, and this might have retarded root growth in the early stage of the experiment. Starting from Day 61, there is a rather high nDR in the B_{v2} horizon, but there are almost no roots observed at −119.5 cm. This nDR may thus be due to vertical water redistribution from the deeper part of the soil to the root zone.

Relationship between Root Length Density and Water Depletion Rate

The RLD and the DR profiles at different times are shown in Fig. 12. We observed that a rather unusual RLD profile emerged in the soil column. At the end of the experiment, the highest density was observed at −70 cm, which was deeper than we expected. It must be noted that our first RLD measurement was at −19.5 cm. Therefore, it is possible that there was first an increase of RLD near the soil surface that could not be observed. The measured RLD distribution is probably related to the WC distribution in the column and to the fact that the lysimeters received no water during the entire growing season. While the top soil dried out, the RLD in the deeper soil horizons increased, causing the nDR to move downward.

Conclusions

We validated three-dimensional ERT-derived moisture contents in a cropped, undisturbed soil column using a global mass balance method and a comparison between and ERT-derived local variability of the soil water content. The global water mass balance of the soil column could be reproduced well by the ERT method. The standard deviation and patterns of the local water content within horizontal cross-sections of the lysimeter that were measured with TDR could be reproduced in the top horizon. However, the observed variability was small and, in the lower horizons, even too small to be able to distinguish it with

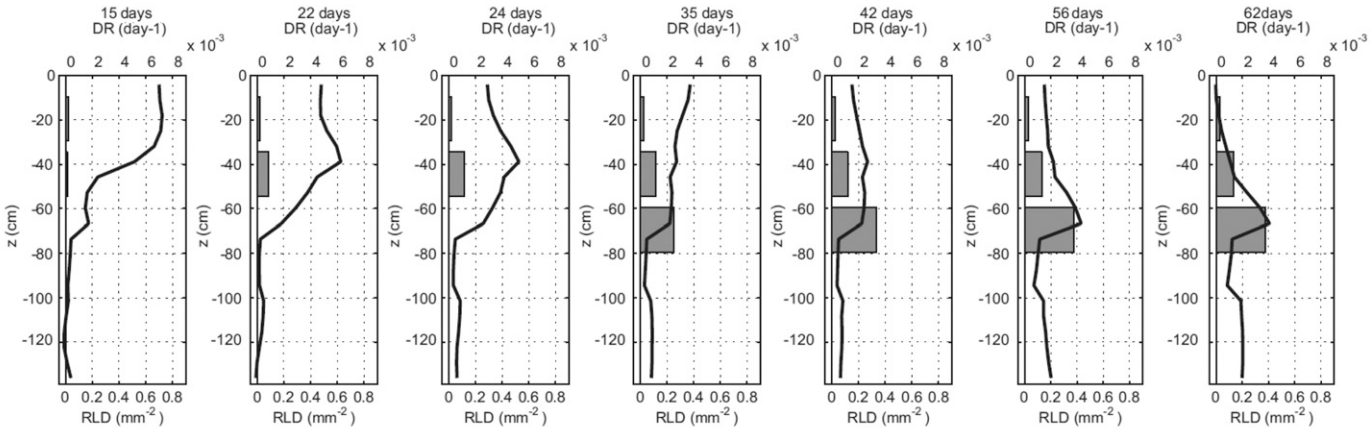

Fig. 12. Water depletion rates (DR, black) and root length density (RLD, gray) profiles after 15, 22, 24, 35, 42, 56, and 62 d.

certainty from noise. These two observations are an important result of the quantitative evaluation of the ERT method. Our analysis sustains the value of this method as a tool to monitor and quantify three-dimensional water content patterns and water content changes in a layered soil.

We have shown that a horizon-specific, in situ calibration of the ERT measurements was necessary to convert the bulk electrical conductivity to water content. However, more research is needed to understand and predict the effect of roots of herbaceous plants on the measured electrical conductivity, since we observed a change in the pedophysical relationship probably due to root shrinkage at the end of the growing season. Additionally, knowledge about the location and shape of soil horizon boundaries proved to be important to improve the result of ERT-derived WC and estimated water depletion rates, especially at interfaces between horizons.

Electrical resistivity tomography proved to be a suitable technique to observe soil water dynamics at the decimeter scale and a promising tool to unravel the relationship between soil redistribution and root water uptake. We observed that the variability of the obtained water content distribution increased during drying until a threshold water content was reached and then decreased again in the top horizon. In the lower horizons, the maximum WC variability was not yet reached. The observed variability was higher than what was expected from the literature, which may be due to spatially variable RWU. The spatial patterns of wetter and drier regions in a horizontal cross-section of the lysimeter changed during the drying process. However, this needs further investigation, since in the literature, both an increase and a decrease of soil moisture variability due to RWU have been reported (e.g., Teuling and Troch, 2005).

Finally, a rather unexpected RLD profile with the maximum root length density at a depth of −70 cm was observed. This observation must be carefully interpreted, since the RLD was only measured at four depths. Nonetheless, it suggests that the root architecture in a layered soil can depend on soil characteristics and dynamically adapt to soil moisture states in the soil profile. Our results indicate that this adaption can be a compensation mechanism for local water shortage in the soil profile.

Acknowledgments

The authors would like to thank Dr. Thomas Pütz and Werner Mittelstaedt for the excavation of the lysimeter, as well as Ansgar Weuthen, Normen Hermes, Ferdinand Engels, and Jürgen Höltkemeier for the technical design and support. This project was financed by the Helmholtz virtual institute "Inverse Modelling of Terrestrial Systems" INVEST.

References

Allen, R.G., L.S. Pereira, D. Raes, and M. Smith. 1998. Crop evapotranspiration—Guidelines for computing crop water requirements. FAO Irrigation and drainage paper 56. FAO, Rome.

Amato, M., G. Bitella, R. Rossi, J.A. Gómez, S. Lovelli, and J.J.F. Gomes. 2009. Multi-electrode 3D resistivity imaging of alfalfa root zone. Eur. J. Agron. 31:213–222.

Amidu, S.A., and J.A. Dunbar. 2007. Geoelectric studies of seasonal wetting and drying of a Texas vertisol. Vadose Zone J. 6:511–523.

Archie, G.E. 1942. The electrical resistivity log as an aid in determining some reservoir characteristics. Trans. Am. Inst. Min. Metall. Pet. Eng. 146:54–67.

Al Hagrey, S.A. 2007. Geophysical imaging of root-zone, trunk, and moisture heterogeneity. J. Exp. Bot. 58:839–854.

Bengough, A.G., M.F. Bransby, J. Hans, S.J. McKenna, T.J. Roberts, and T.A. Valentine. 2006. Root responses to soil physical conditions; growth dynamics from field to cell. J. Exp. Bot. 57:437–447.

Bernier, P.Y., and G. Robitaille. 2004. A plane intersect method for estimating fine root productivity of trees from minirhizotron images. Plant Soil 265:165–173.

Besson, A., I. Cousin, A. Samouëlian, H. Boizard, and G. Richard. 2004. Structural heterogeneity of the soil tilled layer as characterized by 2D electrical resistivity surveying. Soil Tillage Res. 79:239–249.

Binley, A., S. Henry Poulter, and B. Shaw. 1996a. Examination of solute transport in an undisturbed soil column using electrical resistance tomography. Water Resour. Res. 32:763–769.

Binley, A., B. Shaw, and S. Henry Poulter. 1996b. Flow pathways in porous media: Electrical resistance tomography and dye staining image verification. Meas. Sci. Technol. 7:384–390.

Coelho, E.F., and D. Or. 1999. Root distribution and water uptake patterns of corn under surface and subsurface drip irrigation. Plant Soil 206:123–136.

Daily, W., and A. Ramirez. 1995. Electrical resistance tomography during in-situ trichloroethylene remediation at the Savanna River Site. J. Appl. Geophys. 33:239–249.

Daily, W., and A.L. Ramirez. 2000. Electrical imaging of engineered hydraulic barriers. Geophysics 65:83–94.

Descloitres, M., O. Ribolzi, and Y. Le Troquer. 2003. Study of infiltration in a Sahelian gully erosion area using time-lapse resistivity mapping. Catena 53:229–253.

Dubach, M., and M.P. Ruselle. 1995. Reducing the cost of estimating root turnover with horizontally installed minirhizotrons. Agron. J. 87:258–263.

French, H., and A. Binley. 2004. Snowmelt infiltration: Monitoring temporal and spatial variability using time-lapse electrical resistivity. J. Hydrol. 297:174–186.

French, H.K., C. Hardbattle, A. Binley, P. Winship, and L. Jakobsen. 2002. Monitoring snowmelt induced unsaturated flow and transport using electrical resistivity tomography. J. Hydrol. 267:273–284.

Friedel, S. 2003. Resolution, stability and efficiency of resistivity tomography estimated from a generalized inverse approach. Geophys. J. Int. 153:305–316.

Furman, A., T.P.A. Ferre, and A.W. Warrick. 2004. Optimization of ERT surveys for monitoring transient hydrological events using perturbation sensitivity and genetic algorithms. Vadose Zone J. 3:1230–1239.

Garré, S., J. Koestel, T. Guenther, M. Javaux, J. Vanderborght, and H. Vereecken. 2010. Comparison of heterogeneous transport processes observed with electrical resistivity tomography in two soils. Vadose Zone J. 9:336–349.

Gharibi, M., and L.R. Bentley. 2005. Resolution of 3-D electrical resistivity images from inversions of 2-D orthogonal lines. J. Environ. Eng. Geophys. 10:339–349.

Glass, R.J., M.J. Nicholl, A.L. Ramirez, and W.D. Daily. 2002. Liquid phase structure within an unsaturated fracture network beneath a surface infiltration event: Field experiment. Water Resour. Res. 38:1199, doi:10.1029/2000WR000167.

Green, S., and B.E. Clothier. 1999. The root zone dynamics of water uptake by a mature apple tree. Plant Soil 206:61–77.

Green, S.R., M.B. Kirkham, and B.E. Clothier. 2006. Root uptake and transpiration: From measurements and models to sustainable irrigation. Agric. Water Manage. 86:165.

Guenther, T., C. Ruecker, and K. Spitzer. 2006. Three-dimensional modelling and inversion of DC resistivity data incorporating topography. II. Inversion. Geophys. J. Int. 166:506–517.

Heeraman, D.A., P.H. Crown, and N.G. Juma. 1993. A color composite technique for detecting root dynamics of barley from minirhizotron images. Plant Soil 157:275–287.

Heimovaara, T.J. 1993. Design of triple-wire time domain reflectometry probes in practice and theory. Soil Sci. Soc. Am. J. 57:1410–1417.

Hendrick, R.L., and K.S. Pregitzer. 1996. Applications of minirhizotrons to understand root function in forests and other natural ecosystems. Plant Soil 185:293–304.

Henry-Poulter, S. 1996. An investigation of transport properties in natural soils using electrical resistance tomography. Ph.D. diss. Lancaster Univ., Lancaster, UK.

Hupet, F., S. Lambot, M. Javaux, and M. Vanclooster. 2002a. On the identification of macroscopic root water uptake parameters from soil water content observations. Water Resour. Res. 38:1300.

Itoh, S. 1985. In situ measurement of rooting density by micro-rhizotron. Japanese Society of Soil Science and Plant Nutrition, Tokyo, Japan.

Johnson, M.G., D.T. Tingey, D.L. Phillips, and M.J. Storm. 2001. Review: Advancing fine root research with minirhizotrons. Environ. Exp. Bot. 45:263–289.

Katul, G., F. Todd, D. Pataki, Z.J. Kabala, and R. Oren. 1997. Soil water depletion by oak trees and the influence of root water uptake on the moisture content spatial statistics. Water Resour. Res. 33:611.

Kemna, A. 2000. Tomographic inversion of complex resistivity: Theory and application. Der Andere Verlag, Osnabrück.

Koestel, J., A. Kemna, M. Javaux, A. Binley, and H. Vereecken. 2008. Quantitative imaging of solute transport in an unsaturated and undisturbed soil monolith with 3-D ERT and TDR. Water Resour. Res. 44:17.

Koestel, J., J. Vanderborght, M. Javaux, A. Kemna, A. Binley, and H. Vereecken. 2009a. Noninvasive 3-D transport characterization in a sandy soil using ERT: 1. Investigating the validity of ERT-derived transport parameters. Vadose Zone J. 8:711–722.

Koestel, J., J. Vanderborght, M. Javaux, A. Kemna, A. Binley, and H. Vereecken. 2009b. Noninvasive 3-D transport characterization in a sandy soil using ERT: 2. Transport process inference. Vadose Zone J. 8:723–734.

Koumanov, K., J. Hopmans, and L. Schwankl. 2006. Spatial and temporal distribution of root water uptake of an almond tree under microsprinkler irrigation. Irrig. Sci. 24:267–278.

LaBrecque, D.-J., D. Alumbaugh, X.J. Yang, L. Paprocki, and J.R. Brainard. 2002. Three-dimensional monitoring of vadose zone infiltration using electrical resistivity tomography and cross-borehole ground-penetrating radar. p. 259–272. *In* Three-dimensional electromagnetics: Proceedings of the Second International Symposium. Methods in Geochemistry and Geophysics 35. Elsevier, New York.

LaBrecque, D.J., M. Miletto, W. Daily, A. Ramirez, and E. Owen. 1996. The effects of noise on Occam's inversion of resistivity tomography data. Geophysics 61:538–548.

Maillet, G.M., E. Rizzo, A. Revil, and C. Vella. 2005. High resolution electrical resistivity tomography (ERT) in a transition zone environment: Application for detailed internal architecture and infilling processes study of a Rhone River paleo-channel. Mar. Geophys. Res. 26:317–328.

Merrill, S.D., and D.R. Upchurch. 1994. Converting root numbers observed at minirhizotrons to equivalent root length density. Soil Sci. Soc. Am. J. 58:1061–1067.

Michot, D., Y. Benderitter, A. Dorigny, B. Nicoullaud, D. King, and A. Tabbagh. 2003. Spatial and temporal monitoring of soil water content with an irrigated corn crop cover using surface electrical resistivity tomography. Water Resour. Res. 39:1138, doi:10.1029/2002WR001581.

Musters, P.A.D., and W. Bouten. 1999. Assessing rooting depths of an Austrian pine stand by inverse modeling soil water content maps. Water Resour. Res. 35:3041–3048.

Musters, P.A.D., and W. Bouten. 2000. A method for identifying optimum strategies of measuring soil water contents for calibrating a root water uptake model. J. Hydrol. 227:273–286.

Oberdörster, C., J. Vanderborght, A. Kemna, and H. Vereecken. 2010. Investigating preferential flow processes in a forest soil using time domain reflectometry and electrical resistivity tomography. Vadose Zone J. 9:350–361.

Olsen, P.A., A. Binley, S. Henry-Poulter, and W. Tych. 1999. Characterizing solute transport in undisturbed soil cores using electrical and X-ray tomographic methods. Hydrol. Processes 13:211–221.

Revil, A., L.M. Cathles, S. Losh, and J.A. Nunn. 1998. Electrical conductivity in shaly sands with geophysical applications. J. Geophys. Res. Solid Earth 103:23925–23936.

Robinson, D.A., S.B. Jones, J.M. Wraith, D. Or, and S.P. Friedman. 2003. A review of advances in dielectric and electrical conductivity measurement in soils using time domain reflectometry. Vadose Zone J. 2:444–475.

Sanders, J.L., and D.A. Brown. 1978. A new fiber optic technique for measuring root growth of soybeans under field conditions. Agron. J. 70:1073–1076.

Séger, M., I. Cousin, A. Frison, H. Boizard, and G. Richard. 2009. Characterisation of the structural heterogeneity of the soil tilled layer by using in situ 2D and 3D electrical resistivity measurements. Soil Tillage Res. 103:387–398.

Sharp, R.E., and W.J. Davies. 1985. Root growth and water uptake by maize plants. J. Exp. Bot. 36:1441–1456.

Singha, K., and S.M. Gorelick. 2006. Effects of spatially variable resolution on field-scale estimates of tracer concentration from electrical inversions using Archie's law. Geophysics 71:G83–G91.

Singha, K., and S. Moysey. 2006. Accounting for spatially variable resolution in electrical resistivity tomography through field-scale rock-physics relations. Geophysics 71:A25–A28.

Slater, L.D., A. Binley, and D. Brown. 1997. Electrical imaging of fractures using ground-water salinity change. Ground Water 35:436–442.

Slater, L.D., and S.K. Sandberg. 2000. Resistivity and induced polarization monitoring of salt transport under natural hydraulic gradients. Geophysics 65:408–420.

Srayeddin, I., and C. Doussan. 2009. Estimation of the spatial variability of root water uptake of maize and sorghum at the field scale by electrical resistivity tomography. Plant Soil 319:185–207.

Steele, S.J., S.T. Gower, J.G. Vogel, and J.M. Norman. 1997. Root mass, net primary production and turnover in aspen, jack pine and black spruce forests in Saskatchewan and Manitoba, Canada. Tree Physiol. 17:577–587.

Stubben, M., and D. LaBrecque. 1998. 3-D ERT inversion used to monitor an infiltration experiment. p. 593–601. *In* Proceedings of the Symposium on the Application of Geophysics to Environmental and Engineering Problems (SAGEEP), Chicago, IL. Environmental and Engineering Geophysical Society, Wheat Ridge, CO.

Stummer, P., H. Maurer, and A.G. Green. 2004. Experimental design: Electrical resistivity data sets that provide optimum subsurface information. Geophysics 69:120–139.

Taylor, H.M., M.G. Huck, B. Klepper, and Z.F. Lund. 1970. Measurement of soil-grown roots in a rhizotron. Agron. J. 62:807–809.

Teuling, A.J., and P.A. Troch. 2005. Improved understanding of soil moisture variability dynamics. Geophys. Res. Lett. 32:L05404, doi:10.1029/2004GL021935.

Topp, G.C. 1980. Electromagnetic determination of soil water content: Measurements in coaxial transmission lines. Water Resour. Res. 16:574–582.

Vereecken, H., J.A. Huisman, H. Bogena, J. Vanderborght, J.A. Vrugt, and J.W. Hopmans. 2008. On the value of soil moisture measurements

in vadose zone hydrology: A review. Water Resour. Res. 44:W00D06, doi:10.1029/2008WR006829.

Vereecken, H., T. Kamai, T. Harter, R. Kasteel, J. Hopmans, and J. Vanderborght. 2007. Explaining soil moisture variability as a function of mean soil moisture: A stochastic unsaturated flow perspective. Geophys. Res. Lett. 34:L22402.

Vrugt, J.A., J.W. Hopmans, and J. Simunek. 2001a. Calibration of a two-dimensional root water uptake model. Soil Sci. Soc. Am. J. 65:1027–1037.

Vrugt, J.A., M.T. van Wijk, J.W. Hopmans, and J. Simunek. 2001b. One-, two-, and three-dimensional root water uptake functions for transient modeling. Water Resour. Res. 37:2457–2470.

Waxman, M.H., and L.J.M. Smits. 1968. Electrical conductivities in oil-bearing shaly sands. Soc. Petrol. Eng. J. 8:107.

Wells, C.E., and S. Birchfield. 2009. Rootfly: Software for minirhizotron image analysis. Available at http://www.ces.clemson.edu/~stb/rootfly (verified 22 Dec. 2010). Clemson Univ., Clemson, SC.

Werban, U., S.A. al Hagrey, and W. Rabbel. 2008. Monitoring of root-zone water content in the laboratory by 2D geoelectrical tomography. J. Plant Nutr. Soil Sci. 171:927–935.

Zenone, T., G. Morelli, M. Teobaldelli, F. Fischanger, M. Matteucci, M. Sordini, A. Armani, C. Ferre, T. Chiti, and G. Seufert. 2008. Preliminary use of ground-penetrating radar and electrical resistivity tomography to study tree roots in pine forests and poplar plantations. Commonwealth Scientific and Industrial Research Organization, Collingwood, Australia.

Zhou, Q.Y., J. Shimada, and A. Sato. 2002. Temporal variations of the three-dimensional rainfall infiltration process in heterogeneous soil. Water Resour. Res. 38:1030, doi:10.1029/2001WR000349.